RESEARCH PAPER

Thermal and Electrical Characterization of (1-x)Na_2O-xAl_2O_3-P_2O_5 System Glasses

Nihel Hsouna[1], Mohsen Mhadhbi[2,*], Chaker Bouzidi[1]

* *mohsen.mhadhbi@inrap.rnrt.tn*

[1] Laboratory of Physico-Chemistry of Mineral Materials and their Applications, National Center for Research in Materials Sciences, Borj Cedria Technopark, BP 73, 8027 Soliman, Tunisia

[2] Laboratory of Useful Materials, National Institute of Research and Physicochemical Analysis, Technopole Sidi Thabet 2020 Ariana, Tunisia

Received: August 2021 **Revised: October 2021** **Accepted: November 2021**

DOI: 10.22068/ijmse.2413

Abstract: *Phosphate glass with different Al_2O_3 and Na_2CO_3 content [80NaH_2PO_4-(20-x) Na_2CO_3-xAl_2O_3 with a step of 0 to 4] were prepared through melt quenching technique furnace at 900°C. In order to determine the structure and microstructure modification of the samples after heat treatment the IR and Raman spectroscopy were performed. The X-ray diffraction (XRD) result indicated the amorphous nature of the as prepared glass. The result obtained by differential scanning calorimetry (DSC) revealed a good thermal stability in the temperature range of 25 to 400°C. The impedance Nyquist diagrams were investigated and modeled by resistors and constant phase elements (CPE) equivalent circuits. These measurements showed a non-Debye type dielectric relaxation. Both the AC and DC conductivity, dielectric constant, and loss factors were determined. Thermal activation energies were also calculated. A change in the electrical conductivity and activation energy with changes in the chemical composition were observed. Also, a transition in the conduction mechanism from ionic to mixed ionic polaronic was noted. In the same line, electrical modulus and dielectric loss parameters are also deduced. Their frequency and temperature dependency exhibited relaxation behavior. Likewise, activation energies value obtained from the analysis of M'' and those obtained from the conductivity were in close agreement, indicating the optimal character of the preparation conditions.*

Keywords: *Phosphate glasses, Nyquist diagrams, X-ray diffraction, Conductivity, Activation energy, Thermal properties.*

1. INTRODUCTION

Phosphate glasses are a scientific temptation and are prime materials for the development of new analytical techniques, electronic devices such as capacitors [1] and biomedical applications like engineering [2]. Not only because they are easy to produce at low temperatures [3], which leads to a low cost unlike the case of crystalline materials, or because they have a strong added value in the field of optics, magnetic and electrical [4, 5], but also because they can accept several other oxides in very large quantities which allows us to develop and multiply in good conditions their characteristics without risk of disappearance [6]. Adding Al_2O_3 to phosphate glass has been reported to improve their physical properties and chemical stability [7]. On the other hand, Al_2O_3 increases the crosslinking between the PO_4 tetrahedra in the glass which results in a thermally stable and a moisture free glass with a low coefficient of thermal expansion that are used in exchange planar waveguide devices [8]. Another important source of valuable information, on conduction processes, is the study of dielectric properties. Indeed, it makes it possible to understand the origin of the dielectric losses, the electrical and dielectric properties, dipolar relaxation time, its activation losses and its activation energy. In other words, it is advantageous for extracting the overall response of the material because it eliminates the polarization of the electrode and masks the relaxation response due to conduction. The study of the dielectric properties is expected to provide information on the structural aspects of the glasses [9, 10]. Alotaibi et al. [11] fabricated a new P_2O_5-CaO-Na_2O-K_2O-PbO glasses of compositions of 40P_2O_5- 20CaO- (30-x)Na_2O-10K_2O- xPbO and (x= 0, 5, 10, 15, and 20 mol %) (coded as PbP1, PbP2, PbP3, PbP4, and PbP5 for x= 0, 5, 10, 15, and 20 mol %, respectively). The physical and optical properties have been also investigated, and the results showed that PbP5 has the greatest linear attenuation coefficients at all tested energies as well as the best shielding capability. Filho et al. [12] synthesized P_2O_5-Al_2O_3- Na_2O- K_2O phosphate glasses, with

different K_2O/Al_2O_3 ratios, by the melt quenching method. They revealed that increasing the K_2O/Al_2O_3 ratio could control the value of the temperature coefficient of the optical path (ds/dT) to attain the athermalization. In addition, the absorption spectra of the phosphate glasses revealed no marked changes in the optical band gap energy.
In this work, we have prepared phosphate glasses with different concentrations of aluminum oxide to improve the thermal, electrical, and dielectric properties, which could be used for micro batteries.

2. EXPERIMENTAL PROCEDURE

Phosphate glasses were prepared according to the following compositions (with x= 0, 1, 2, 3, and 4 mol %), and were synthesized via a melt quenching technique. The samples are noted by $VPAl_0$, $VPAl_1$, $VPAl_2$, $VPAl_3$, and $VPAl_4$ for x= 0 - 4 mol % Al_2O_3 content, respectively. All the starting chemical constituents are more than 99.9% in purity. Calculated quantities of the chemical components were mixed and ground in mortar batches of high purity, and melted in an electric furnace at 900°C during 1.5 hours in platinum crucible so that a homogeneously-mixed melt was obtained. From this temperature, quenching was done and which consists of rapidly pouring the molten mixture in air into a steel mold previously heated to 200ºC in order to avoid thermal stresses (which can cause the sample to break). The obtained glass is then annealed for two hours in the oven to remedy the stresses created during the casting and obtaining glasses with a good thermal stability at a temperature below 200°C, then a slow return to room temperature.
All glasses were investigated by X-ray diffraction (XRD). The patterns were recorded on a few milligrams of glasses ground in the form of powders at room temperature. The apparatus used in this study is a Panalytical X'Pert Pro diffractometer equipped with a copper anticathode (λ= 1.5418 Å). The angle 2θ varying between 5 and 80° in step size of 0.02°. DSC scans of as-cast glass specimens were carried out in Metler Toldo DSC823e and recorded using few milligrams as-cast glass specimens which were powdered in order to determine the characteristic glass transition temperatures, T_g, crystallization onset, T_x, the melting temperature, T_m, and heated in a platinum crucible using the same amount of alumina powder as reference material with heating rates of 10°C/min between -180 and 700°C temperatures range.
IR spectrum has been recorded by a Perkin Elmer (FTIR 2000) spectrometer in the range of 4000-400 cm^{-1}. The Raman spectrum was registered using HORIBA Scientific (labRAM HR) spectrometer. The samples were excited at 632 nm by He-Ne laser. For the electrical measurements, we used an impedance analyzer (Agilent 4294 A) to get complex impedance data in the frequency range from 10 Hz to 13 MHz at room temperature. For these measurements, different disk-shaped pieces of glass with a diameter of 13 mm and a thickness of 1.5 mm are obtained.

3. RESULTS AND DISCUSSION

3.1. X-ray diffraction results

XRD patterns of the prepared glasses are shown in Figure 1, where the structural evolution of the phases is clearly presented. We can see that all the patterns are unresolved and wide. In addition, no fine diffraction peak is observed on the recorded pattern so the long distance order is absent, which is the characteristic of amorphous materials.

Table 1. Chemical compositions of all examined glasses.

Chemical composition (g) / Sample	$NaPO_4.2H_2O$	Al_2O_3	Na_2CO_3
$VPAl_0$	8.9295	-	1.0705
$VPAl_1$	8.9318	0.06869	0.9994
$VPAl_2$	8.9342	0.1374	0.9282
$VPAl_3$	8.9367	0.2062	0.8571
$VPAl_4$	8.9400	0.2750	0.7860

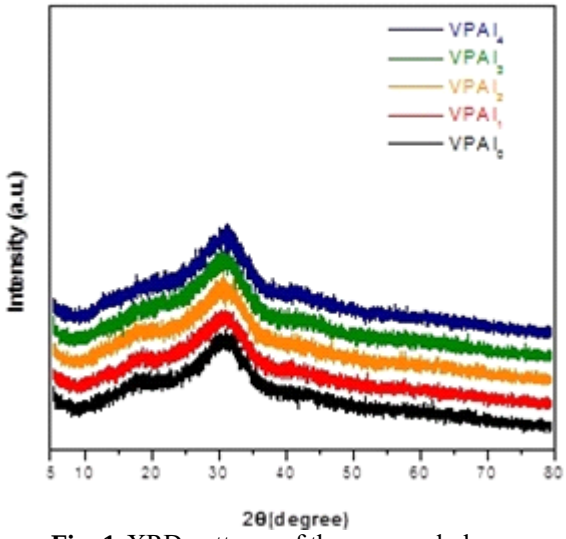

Fig. 1. XRD patterns of the prepared glasses.

3.2. Raman analysis

Figure 2 shows the Raman spectrum of the glass sample VPAl4 in the frequency range 100-1250 cm^{-1}. The key features of the Raman spectrum of aluminum phosphate glasses are the low frequency attributed to the faint band at 339 cm^{-1}, which can be assigned to the deformation modes of (O-P-O) [13].

Bands situated at 509 and 699 cm^{-1} are related to the deformation modes of (P-O-P) and the asymmetric stretching vibration P-O-P bridging bonds in the little phosphate unit, respectively. The broad band at about 891 cm^{-1} could be attributed to the symmetric stretching vibrations in $(PO4)^{3-}$ tetrahedral chains [14]. The bands near 1046 and 1157 cm^{-1} are assigned to the asymmetric stretching modes of the (P-O-P)as and (O-P-O)as, respectively [13, 15].

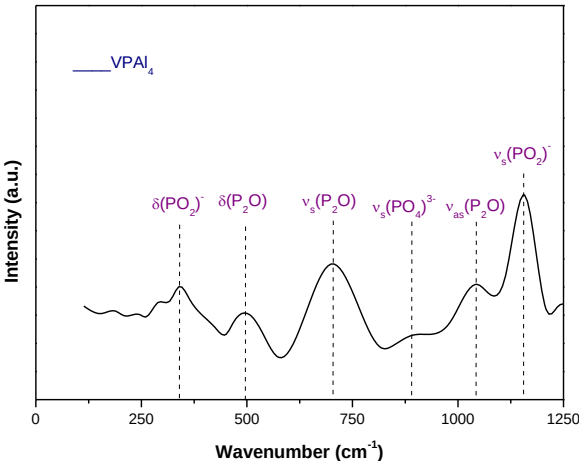

Fig. 2. Raman spectrum of the sample $VPAl_4$.

3.3. FTIR analysis

Figure 3 shows the FTIR spectra, in the frequency range between 400 and 4500 cm^{-1}, of the samples. They are similar to those reported for other phosphate glasses [16]. The band at 3311 cm^{-1} is assigned to correspond to the vibrations of hydroxyl groups (OH^-) in vitreous materials [17]. The absorption band 1663 cm^{-1} is assigned to asymmetric stretching mode of the two non-bridging oxygen atoms bonded to phosphorus atoms, the O–P–O or (PO_2) as units [18]. Moreover, the absorption band 1252 cm^{-1} is asymmetric stretching vibration of O–P–O or (PO_2) as units, in the phosphate tetrahedral [18]. The band at around 1090 cm^{-1} is attributed to deformation modes of $(PO_4)^{3-}$ groups [19]. The band at about 867 cm^{-1} is asymmetric stretching vibration of P-O-P [20]. The absorption bands near 763 and 705 cm^{-1} are assigned to the asymmetric stretching and the symmetric stretching modes of the in-chain P-O-P linkages, (P-O-P) as and (P-O-P)str, respectively [20, 21]. At low frequency, the spectra show an absorption band near 507 cm^{-1} attributed to the deformation modes of (P-O-P) [13, 17, 18, 22, 23]. On the other hand, all the intensities bands increase with Al_2O_3 amount. The result reveals an increase of non-bridging oxygen (NBO) group, which implies an increase in the chemical durability of the glass network [19, 26, 24].

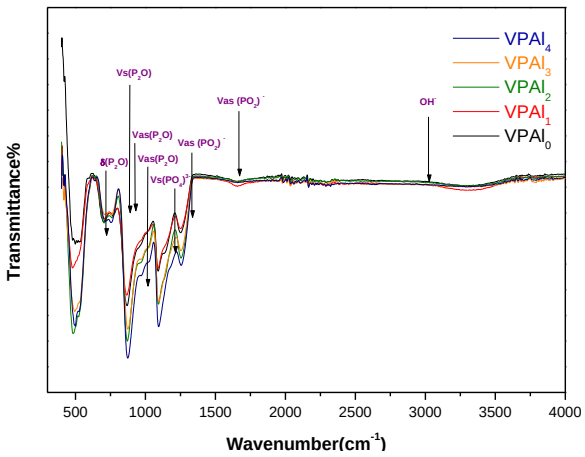

Fig. 3. FTIR spectra of all examined glasses.

3.4. Thermal stability

The Hruby parameter (Kgl) was determined to determine the glasses stability [25]. This parameter can be also used as a quick measure of

glass-forming tendencies of materials. Figure 4 reveals the DSC curves of the phosphate glasses based on P_2O_5 and Na_2O pure and substituted with Al_2O_3 with different molar compositions. Table 2 shows the glass transition (T_g), the crystallization (T_x), the melting temperatures (T_m), and the Hruby parameter Kgl= $(Tx-T_g)/(T_m-T_x)$. Good glass forms are characterized by high values of Kgl and vice-versa. We noticed that Kgl predominates for x= 2% mol, then there is a safety margin to prevents devitrification.

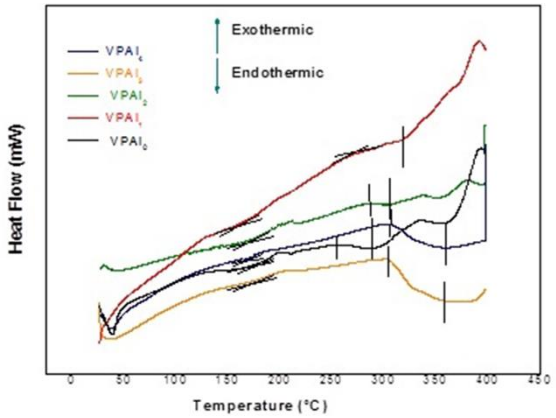

Fig. 4. DSC curves of the prepared glasses.

Table 2. Thermal parameters of the prepared glasses.

Sample	T_g(°C)	T_x(°C)	T_m(°C)	K_{gl}(°C)
$VPAl_0$	171.35	255.33	289.08	2.48830
$VPAl_1$	171.35	284.51	317.57	3.42287
$VPAl_2$	171.35	288.19	305.26	6.84476
$VPAl_3$	171.35	303.97	355.99	2.54940
$VPAl_4$	171.35	305.56	359.76	2.47620

3.5. Impedance spectroscopy

3.5.1. Nyquist spectra

As it is well-founded, electronic and ionic contributions are primarily responsible for electrical conductivity. The first follows the theory of hopping while the second is due to ionic concentration and mobility [26, 27]. Nyquist representations are used to analyze the electrical and dielectric properties of samples. Figure 5 shows the impedance diagrams, plotted in the Nyquist plane, obtained for $VPAl_0$, $VPAl_1$, $VPAl_2$, $VPAl_3$, and $VPAl_4$ at a temperature of 100°C. In the beginning, we considered that each semicircle is equal to a circuit composed of two parallel RC elements connected in series [28]. These curves show a single semi-circle in the frequency domain studied. The centers of the half-arcs lie below the Z′ axis, which suggests that the relaxation is of the non-Debye type. For this reason, it is better to replace the capacitor with the phase constant element (CPE), so as to account for the arc compression [28]. This behavior indicates that the electrical response at complex plane impedance presents a non-Debye relaxation [29, 30]. A good agreement between the experimental and theoretical values is obtained, which proves that the electrical properties of glass samples are adequately defined with the proposed equivalent circuit.

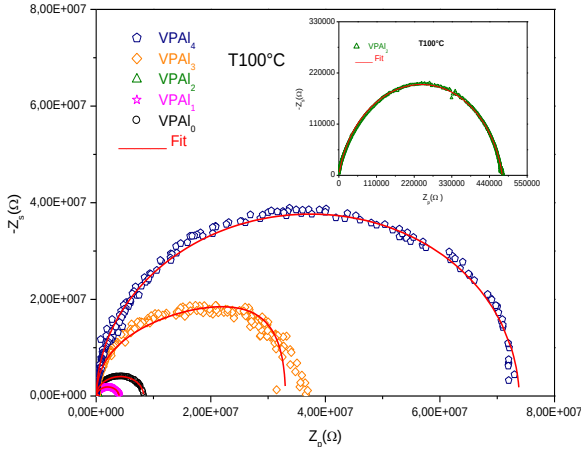

Fig. 5. Experimental and theoretical impedance diagrams of the samples. Inset: impedance diagrams of the sample $VPAl_2$ at T= 100°C.

Thus, the total impedance of the equivalent circuit is given by:

$$Z^* = Z' + jZ'' = \left[\frac{1}{R_b} + \frac{1}{Z^*_{CPE}}\right]^{-1} \quad (1)$$

where Z' and Z'' are the real and imaginary components of impedance, respectively. The impedance of the CPE is defined by [31]:

$$Z^*_{CPE} = \frac{1}{A_0 (j\omega)^n} \quad (2)$$

where j is the imaginary unit (j_2= 1) and v the angular frequency (v= 2πf, f is the frequency), A being a constant independent of frequency [26]. n, a dimensionless parameter between 0 and 1. This latter determines the degree of deviation from an exact semicircle. When n= 1, Eq. (2), the CPE behaves like an ideal capacitor, where A_0= C, which is the case with typical Debye

behavior. If n= 0, the CPE acts like a pure resistance and takes the value R= 1/A. The calculation of the parameter n is described in [32]. R_b and A_0 refer to the resistive and capacitive components of the ground region, respectively.
Based on the following relationships (3) and (4), the diagrams of Nyquist plots are fitted with the ORIGIN6.0 software:

$$Z' = \frac{R_b \times \left(1 + R_b A_0 \omega^n \times \cos\left(\frac{n\pi}{2}\right)\right)}{1 + 2R_b A_0 \omega^n \times \cos\left(\frac{n\pi}{2}\right) + \left(R_b A_0 \omega^n\right)} \quad (3)$$

$$Z'' = \frac{R_b^2 A_0 \omega^n \times \sin\left(\frac{n\pi}{2}\right)}{1 + 2R_b A_0 \omega^n \times \cos\left(\frac{n\pi}{2}\right) + \left(R_b A_0 \omega^n\right)} \quad (4)$$

The simulation results are collected in Table 3. It is found that the values of bulk resistance (R_b) decrease gradually with the increase of the concentration of Al_2O_3 (up to 2 % mol) followed by an increase beyond this value. We can conclude an increase in polaronic conductivity, which leads to a decrease of the bulk resistance, R_b, with the increase in temperature at a constant concentration. On one hand and by the low values of the sample $VPAl_2$ compared to the rest of the samples at a constant temperature, confirmed by the remarkable decrease of the semicircle in the Nyquist diagram of the sample $VPAl_2$ and its shift to higher frequencies (Table 3).
Figure 6 illustrates the typical complex impedance curves at several temperatures of $VPAl_2$. The obtained plot shows that, when the temperature increases, the maximum imaginary impedance spectra (Z_s) shifts to the high frequency side of the abscissa and the arc corresponding to the bulk resistance of the pattern decreases. This was explained by an activated thermal conduction mechanism in the literature [33, 34].

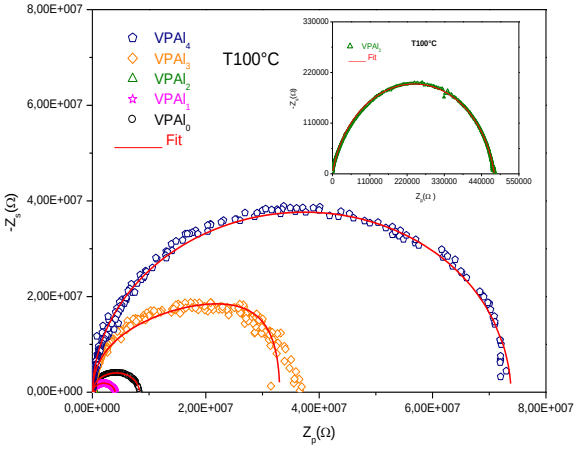

Fig. 6. Experimental impedance diagrams of the samples at different temperature.

3.5.2. Impedance analysis

The variation of real and imaginary parts of impedance for $VPAl_2$ (2 mol% Al_2O_3) glasses as a function of the frequency at different temperatures are illustrate in Figure 7.a and Figure 7.b, respectively. The theoretical curve fitting and experimental data are measured. Furthermore, a good agreement between the experimental and theoretical curves was revealed. We observed that the real part of the impedance Z' gradually decreases with temperature. This decrease can be interpreted by the presence of space load zone following the reduction in the resistive behavior of the material. The curves show that the values of Z″ reach maxima Z''_{max} and these values shift with widening towards higher frequencies with the increase in temperature. The displacement and widening of the Z″ peaks as a function of frequency confirms the existence of a possible relaxation phenomenon [35]. It is noted that the maximum imaginary impedance spectrum Z" passes at high frequency, with an increase in temperature, in which the resistance of the sample decreases which confirms the increase in electrical conductivity [36-38].

Table 3. The best fitting values of equivalent circuit elements for different glass samples.

Temperature (°C) Resistance (Ω)	25	50	100	150	200	250
R_b ($VPAl_0$)	-	1.18562E7	8.3647E6	1.19653E6	407653.701	226751.359
R_b ($VPAl_1$)	-	1.57601E7	4.01776E6	563910.345	107429.467	48388.71
R_b ($VPAl_2$)	1.73045E6	1.16742E6	475862.069	559057.4713	48218.3908	16269.5925
R_b ($VPAl_3$)	-	-	3.6698E7	2.57116E7	4.68046E6	787523.511
R_b ($VPAl_4$)	-	-	7.41149E7	1.64548E7	1.05379E7	9.69195E6

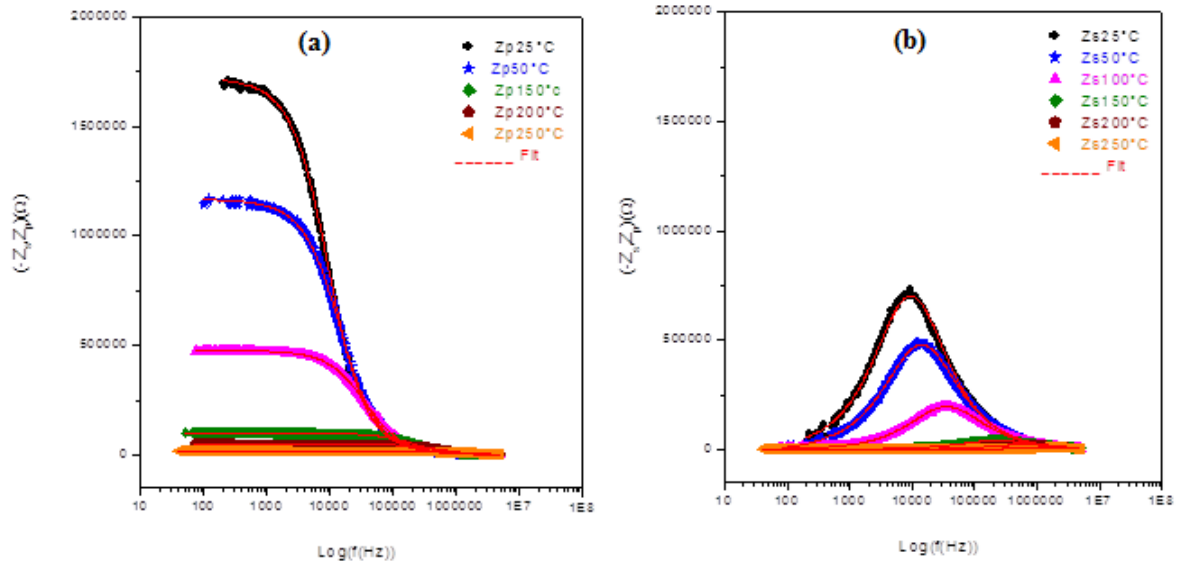

Fig. 7. Variation of (a) real part of impedance (Z') and (b) imaginary part of impedance (Z'') as a function of frequency at different temperature of $VPAl_2$.

3.5.3. *Conductivity analysis*

3.5.3.1 *DC electrical conductivity*

The measured values of impedance were used to study the behavior of AC conductivity of the prepared phosphate glasses were calculated by using the following relation [39]:

$$\sigma = \frac{e}{S}\frac{Z'}{Z'^2 + Z''^2} \quad (5)$$

where e is the sample thickness and S is the electrode area used to measure the properties of the sample. The effect of temperature and concentration on conductivity are plotted in Figure 8 and Figure 9, respectively.

We can conclude a predominance of the electronic conductivity for x= 2 % mol, which is confirmed by the minimum radius of the arc corresponding to bulk resistance of the prepared sample.

From these figures we notice that there are two types of highlighted behaviors: the first behavior, in the form of a plateau that extends over low frequencies that can be attributed to the long-distance transport of mobile Al ions in response to the applied electric field, corresponds to direct current conductivity ($\sigma = \sigma_{DC}$).

The second behavior exhibits dispersion at higher frequencies, which can be attributed to the microscopic nature of the inhomogeneities with the distribution of the relaxation phenomena following the reduction in the resistive behavior of the material by reducing its barrier [40, 41]. The effect of temperature on conductivity is plotted in Figure 8, which shows that the conductivity varies with temperature according to Arrhenius equation:

$$\sigma_{DC} = \frac{A}{T}\exp\left(-\frac{Ea}{k_B T}\right) \quad (6)$$

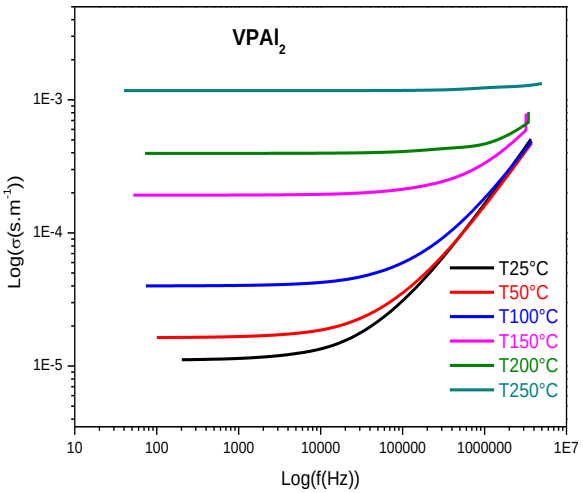

Fig. 8. Variation of the AC conductivity of $VPAl_2$ glass versus frequency at different temperatures.

where E_a is the activation energy, A is constant, k_B is the Boltzmann constant, and T is the temperature.

Arrhenius plots of the variation of DC conductivity for the prepared glass samples, with the temperature in the range of 323-523 K, are shown in Figure 10. The activation energy values can be deduced from the logarithmic variation of

conductivity Ln(σ_{DC}T) as a function of 1000/T. It is observed that the conductivity of the glass sample can be well adjusted by a straight line increasing linearly with increasing temperature. The calculated activation energies for all the Al_2O_3 compositions are illustrated in Figure 11.

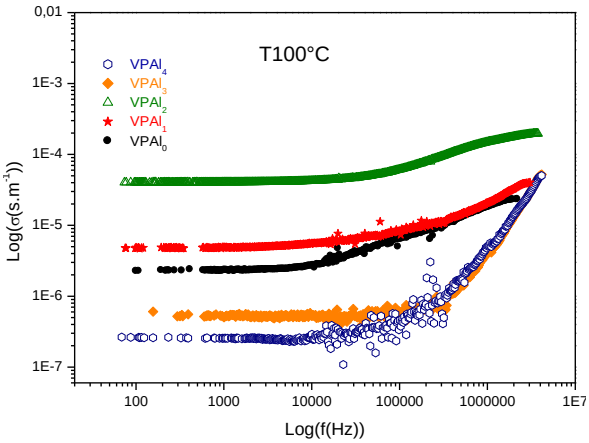

Fig. 9. Variation of the AC conductivity of $VPAl_2$ glass versus frequency at different concentrations.

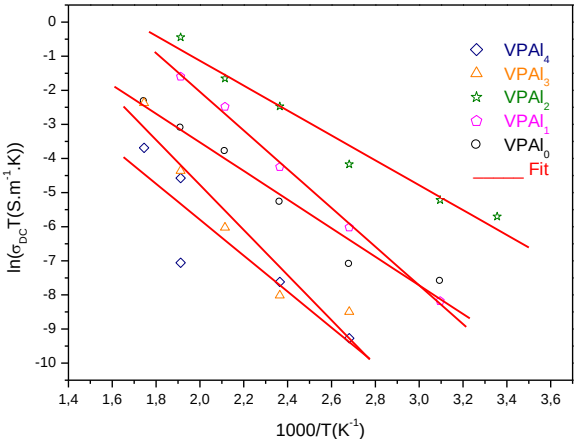

Fig. 10. Arrhenius relation of Ln(σ_{dc}×T) versus 1000/T for all samples.

It can be seen that with the increasing of alumina content the activation energy changes in the range of 0.31-0.57 eV. Hence, we revealed a non-linear behavior of the conductivity. The result may be explained by a competition between electronic and ionic conduction type. We may therefore conclude that the electronic conductivity was predominant to 1< x< 2 mol.% and 3< x< 4 mol.%, and an ionic conductivity operates for 0< x< 1 mol.% and 2< x< 3 mol.%. Results are previously reported in zincovandophosphate glasses and sodium vanadophosphate glasses [42, 43]. The addition of Na^+ to the first (P_2O_5) modifies the network creating non-bridging oxygen (NBO) also in the structure and creates anionic sites with different binding energies of alkali ions and this is confirmed by the energy values activation rate (E_a) obtained for the glass samples. Like crystals, ionic conductivity can be described by the movement of ionic defects [44].

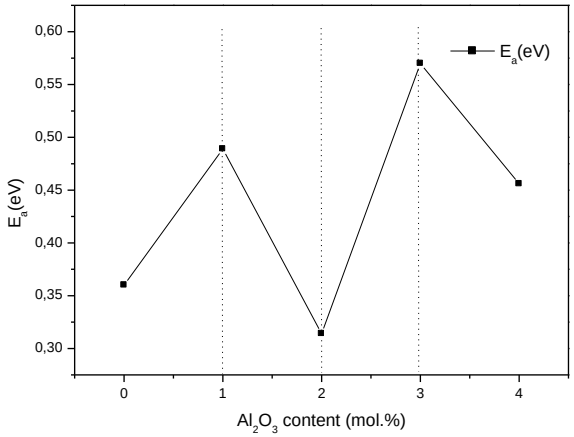

Fig. 11. Variation of activation energy for all the samples.

In fact, there are two path conduction mechanisms: the first one is due to the exchange interaction of Al^{3+}- O -Al^{4+} chains and the other one is due to the creation ions by the regular position of non-bridging oxygen along the chains forming the network [45, 46]. In addition, increasing the aluminum content can cause a stronger colombic attractive force between ions and polarons, which leads to a reduction in electronic and ionic motion [47]. This result is in a mismatch variation of the resistance of the mass region and of the interfacial contribution giving competition between polaronic and ionic conduction in the glass lattice. Therefore, there are NBOs in the pyrophosphate groups that promote ionic conduction [48] and also the vibrations of the oxygen bridges within the Al^{3+}- O -Al^{5+} bonds that promote the conduction of small polaron hopping (SPH) in the glass [49, 50]. The increase in the population of the polaronic component Al_2O_3 imposes the predominance of polaronic conduction. The existence of ion-polaron conduction in glasses is of great interest in electrochemical devices [51].

In fact, polarons have been formed from holes in the valence band where charge carriers inducing strongly localized lattice distortions form a conduction of "small" polarons [52, 53]. The low

value of activation energy for 2 mol % Al_2O_3 can be explained by the dominance of ionic conduction. The change of the conduction mechanism has been also detected in zinc vanadophosphate and silver vanadium tellurite glasses [42, 54]. The activation energy values were shown at different Al_2O_3 concentrations and also compared to other glasses (Table 4). We note that the activation energy of the conductivity of $VPAl_2$ is lower than that of mixed sodium phosphate glasses NPP5 (E_a= 1.54 eV) [55], lithium phosphate glasses (E_a= 1.64 eV) [56], MgO doped ZnO-P_2O_5 [57] and lithium bismuthate glasses ((75-x)Bi_2O_3-10ZnO-15B_2O_3-(x)Li_2O, x= 5, 10, 15, 20 mol %)(1.29-1.35 eV) [58]. Besides, the obtained values of E_a are near borophosphate glasses PBF_4 (0.54 eV) [59] and lithium niobium silicate glasses SLND [60].

Table 4. Values of activation energy for different composition of glasses.

Sample code	E_a (eV)
0	0.36
1	0.489
2	0.314
3	0.57
4	0.456
Li_2O-P_2O_5 [56]	1.64
CZ13 [57]	1.13
PBF_4 [59]	0.54
SLND [60]	0. 43
BaW1 [61]	1.08

3.5.3.2 Dielectric analysis

The complex permittivity formalism has been employed to reveal significant information about the chemical and physical behavior of the electrical and dielectric properties. It is expressed as [62, 63]:

$$\varepsilon^*(\omega) = \varepsilon'(\omega) - j\varepsilon''(\omega) = \frac{1}{j\omega C_0 (Z' + jZ'')} \quad (7)$$

where ε' and ε'' are the real parts known as the dielectric constants and the imaginary parts is known as the dielectric loss of the complex permittivity. These parameters depend on the frequency. Where C_0 is the capacitance of the empty cell, ε_0 is the permittivity of the vacuum (8.854×10^{-12} Fm^{-1}), A is the cross-sectional area of the flat surface of the pellet (7.853×10^{-5} m^2), and e is its thickness (1.5 mm). Z' is the real part of impedance and Z'' is its imaginary part. From the values of the dielectric constant, we can determine the loss factor tangent given by [64]:

$$\tan(\delta) = \frac{Z'}{Z''} = \frac{\varepsilon''}{\varepsilon'} \quad (8)$$

Hence, we determined the variation of the dielectric constant with the frequency for $VPAl_0$, $VPAl_1$, $VPAl_2$, $VPAl_3$, and $VPAl_4$ glasses at T= 100°C is depicted in inset of Figure 12.

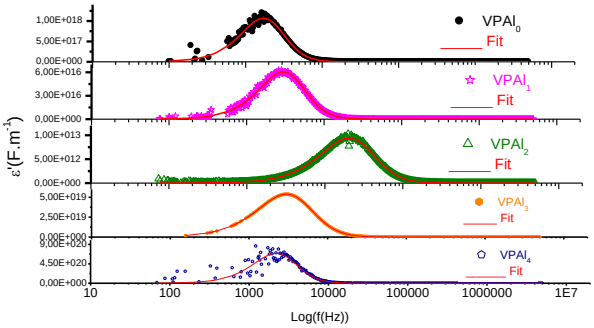

Fig. 12. The frequency dependence curves of dielectric constant ε′(ω) for $VPAl_0$, $VPAl_1$, $VPAl_2$, $VPAl_3$ and $VPAl_4$ glasses at T= 100°C.

There is more variation in the dielectric constant values at low frequency, and they remain constant at high frequency. Thus, there is a significant increase in the value of the dielectric constant in the low frequency region. This can be explained on the basis of the polarization mechanism existing in the sample. Furthermore, the increased dielectric constant value at the low frequency region is related to the contribution from space charge/interfacial polarization. The constant decrease at high frequencies is attributed to the existence of space charge polarization. The space charges can move under the application of an external field and when they are trapped by the defects, lots of dipole moments (space charge polarization) are formed [65].

The frequency dependence of the loss factor tan(δ) are studied for the VPA_l glasses with different concentrations of Al_2O_3 and at T= 100°C as a function of logarithmic frequency at different temperatures shown in Figure 13. We observe that the dielectric loss tan(δ) at low frequency takes relatively high values and increases by increasing the temperature. This is a normal behavior in oxidized glasses and it decreases with the increase of frequency, and this is due to the long-range polaron hopping contribution of mobile ions relative to the immobile glass matrix [38]. This increase in tan(δ) for $VPAl_2$ glass, in the low

frequency region and at higher temperature, may be due to the application of the field which assists the jump of electrons between two different sites in the glasses. The jump on the frequency of charge carriers at high temperatures becomes large and comparable to the frequency of the applied field. This leads to a sharp polarization and gives an increase in dielectric constant and loss factor [66]. As a result, charge carriers easily jump off sites with high free energy barriers. In the high frequency region, the dielectric loss tan(δ) is fairly constant. The dielectric constant and the factor loss both approximate constant values which results from the rapid polarization processes occurring in the glasses under an applied field [67]. However, at high frequencies, the charge carriers will no longer be able to spin fast enough, so their oscillation will start to lie behind this field, causing the dielectric constant and loss factor to decrease. At low temperature, the jump frequency of the transported load becomes lower than the frequency of the applied field.

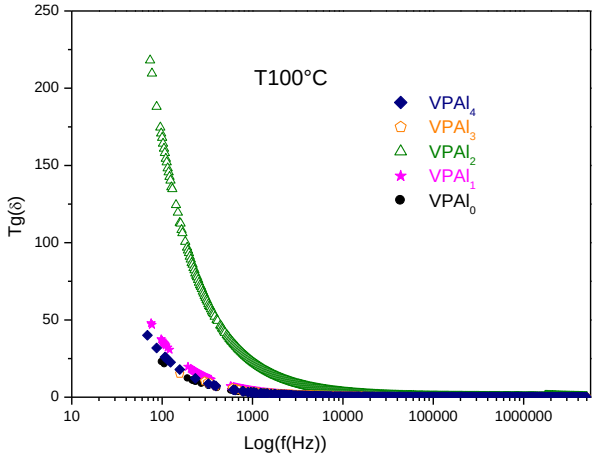

Fig. 13. The frequency dependence curves of loss factor for the prepared glasses at T= 100°C.

The electrical modulus formalism was used for a better description of the dynamic processes in the present glass system. This formalism is appropriate to identify phenomena such as electrode polarization and bulk phenomenon, such as average conductivity relaxation times [68].

$$M^* = \frac{1}{\varepsilon^*(\omega)} = M'(\omega) + jM''(\omega) \quad (9)$$

The imaginary and real parts of the electric modulus were obtained from the impedance data according to the following equation:

$$M'(\omega) = \omega C_0 Z'' \quad (10)$$

and

$$M^*(\omega) = \omega C_0 Z' \quad (11)$$

where C_0 is the vacuum capacitance of the cell. Figure 14 shows the real M' and imaginary M'' parts of the electrical modulus for the $VPAl_2$ sample at various temperatures as a function of frequency, respectively. The real part of the electrical modulus M' tends to zero at low frequency and reaches a maximum at high frequency side for all temperatures. This phenomenon may be due to the short range mobility of charge carriers and the increase of the migration of conducting ions [69]. Moreover, at high frequency, the real part (M') decreases and such behavior was explained by the accumulation of charges between the sample and the electrode at the interface. It can be attributed to the fact that at high frequency the electric field changes so rapidly that the ions can move only within their potential wells [70]. The imaginary part (M'') shows an asymmetric peak at some temperatures, the peak in the imaginary part of the modulus is found to be shifted towards higher frequencies with the increase of the temperature and this is related to the thermally activated ion dynamics of the glass. The presence of relaxation-peaks in the M'' plot indicates that the samples are ionic conductors [71].

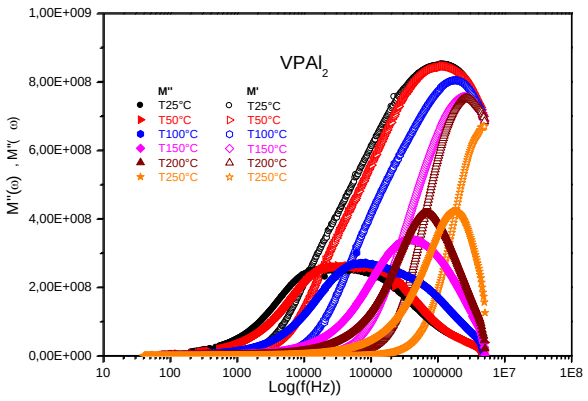

Fig. 14. The frequency dependence of M' and M'' for $VPAl_2$ sample at different temperatures.

The spectra describe two regions: the frequency region below f_{max} determines the range in which charge carriers are mobile over long distances and it is due to the hopping of ions, and for the region above f_{max}, the carriers are confined to potential wells and are mobile over short distances associated with polarization process [72].

The behavior of the sample was studied by plotting the normalized parameters (M''/M''_{max} as a function of log (f/f_{max}), f_{max} is the frequency corresponding to M''_{max}) at different temperatures. The coincidence of all curves in a single reference curve indicates that the temperature is a common relaxation mechanism in these glasses for a specific temperature range [73].

The frequency corresponding to the peak M''_{max} of M'' denoted as f_{max} is given by the condition $\omega \tau = 1$ where the relaxation time is defined as:

$$\tau = \frac{1}{\omega} = \frac{1}{2\pi f_{max}} \quad (12)$$

Figure 15 shows the variation of the relaxation time with the temperature for 2 mol% $VPAL_2$ as represented, which follows the relation [74]:

$$\tau_f = \tau_0 \exp\left(\frac{E_{re}}{k_B T}\right) \quad (13)$$

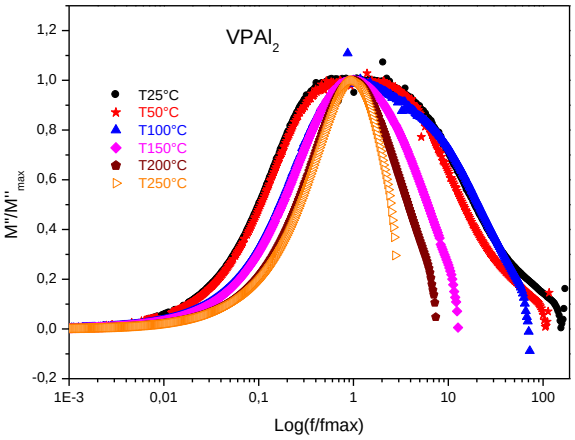

Fig. 15. Variation of M''/M''_{max} as a function of log (f/f_{max}) at different temperature for $VPAl_2$ sample.

where τ_0 is the pre-exponential factor and E_{re} is the activation energy for the conductivity relaxation. Fig. 14 explains how the relaxation time decreases with the elevation in the temperature as a result of the increase in the charge carrier mobility. The relaxation energy is estimated from the linear fitting to be E_{re}= 0.323 eV which is equal to the value of activation energy (E_a= 0.314 eV) calculated from the plot $Ln(\sigma_{DC} \times T)$ vs. 1000/T, which means that the distribution of the random energy barrier is isotropic for charge carriers hopping in the glass.

4. CONCLUSIONS

Phosphate glasses were successfully prepared by melt quenching. The XRD results demonstrated the amorphous nature of all the samples. The trends of variations in conductivity and activation energy with Al_2O_3 content reveals the possibility of competition between electronic and ionic conduction type. Enhanced conductivity was observed with the addition of Al_2O_3 to the $VPAl_2$ glass. The movement of the peak to a higher frequency of ε' for the $VPAl_2$ glass result in an attenuation of the frequency interval in which the jump frequency of the carriers is large and comparable with the frequency of the applied field. This leads to a clear polarization for a wide range frequency. The increase in tan δ in lower frequency, for the $VPAl_2$ glass, may be due to the application of the field, which assists electron hopping between two different sites in the glasses. A relaxation process time for mobile ions resulting from the hop in the random energy barriers, and the extracted values of the activation energies are obtained from the analysis of M''. Based on these results, we conclude that the prepared glass systems could be a suitable host for optical amplifiers from the standpoint of high dielectric constant and good AC electrical conductivity. These characteristics allow our new lens to be a good candidate in nonlinear optical applications.

REFERENCES

[1] Bih, L., Bih, H., Amalhay, M., Mossadik, H., Elbouari, A., Belhorma, B., Graça, M. P. F., Valente, M. A., "Phosphate glass-glasses as new energy density dielectric materials" Procedia Eng., 2014, 83, 371-377.

[2] Abou Neel, E. A., Salih, V, Knowles, J. C., "1.18 Phosphate-based glasses" Compr. Biomater. II, 2017, 1(1), 392-405.

[3] Deepa, A. V., Murugasen, P., Muralimanohar, P., Kumar, S. P., "Optical studies of lanthanum oxide doped phosphate glasses" Optik, 2018, 160, 348-352.

[4] Shelby, J. E., Introduction to Glass Science and Technology, Royal Society of Chemistry, Cambridge, UK, 1997.

[5] Elliot, S. R., Physics of Amorphous Materials, Longman, New York, 1984.

[6] Yariv, A., Yeh, P., Photonics Optical Electronics in Modern Communications,

6th ed., Oxford University Press, USA, 2006, 30-31.

[7] Sreedhar, V. B., Basavapoornima, C, Jayasankar, C. K., "Spectroscopic and fluorescence properties of Sm^{3+} - doped zincfluorophosphate glasses" J. Rare Earths, 2014, 32 (10), 918-926.

[8] Seneschal, K., Smektala, F., Jiang, S., Luo, T., Bureau, B., Lucas, J., Peyghambarian. N., "Alkaline-free phosphate glasses for ultra compact optical fiber amplifiers at 1.5 μm" J. Non-Cryst. Solids, 2003, 324, 179-186.

[9] Murali Krishna, G., Veeraiah, N., Venkatramaiah, N., Venkatesan, R., "Induced crystallization and physical properties of $Li_2O–CaF_2–P_2O_5$:TiO_2 glass system: Part II. Electrical, magnetic and optical properties" J. Alloys Compd., 2008, 450, 486-493.

[10] Sahaya Baskaran, G., Ramana Reddy, M. V., Krishna Rao, D., Veeraiah, N., "Dielectric properties of PbO-P_2O_5-As_2O_3 glass system with Ga_2O_3 as additive". Solid State Commun., 2008, 145, 401-406.

[11] Alotaibi, B. M., Sayyed, M. I., Kumar, A., Alotiby, M., Sharma, A., Al-Yousef, H. A., Alsaif, N. A. M., Al-Hadeethi, Y., "Optical and gamma-ray shielding effectiveness of a newly fabricated P_2O_5-CaO-Na_2O-K_2O-PbO glass system". Progress in Nuclear Energy, 2021, 138, 103798.

[12] Filho, J. C., Zilio, S. C., Messias, D. N., Pilla, V, Silva, A. C. A., Dantas, N. O., Andrade, A. A., "Effects of aluminum substitution by potassium in the P_2O_5-Al_2O_3-Na_2O-K_2O phosphate glasses", J. Alloys Compd., 2020, 815, 152359.

[13] Belharouak, I., Parent, C., Tanguy, B., Le Flem, G., Couzi. M., "Silver aggregates in Photoluminescent phosphate glasses of the Ag_2O-ZnO–P_2O_5 system", J. Non-Cryst. Solids, 1999, 244(2), 238-249.

[14] Frost, R. L., "An infrared and Raman spectroscopic study of natural zinc phosphates", Spectrochim. Acta A, Part A: Mol. Biomol. Spectrosc., 2004, 60, 1439-1445.

[15] Videau, J. J., Portier, J., Piriou, B., "Raman spectroscopic studies of fluorophosphate glasses", J. Non-Cryst. Solids, 1982, 48(2), 385-392.

[16] Yung, S. W., Hsu, S. M., Chang, C. C., Hsu, K. L., Chin, T. S., Hsiang, H. I., Lai, Y. S., "Thermal, chemical, optical properties and structure of Er^{3+}- doped and Er^{3+}/Yb^{3+}- codoped P_2O_5-Al_2O_3-ZnO glasses", J. Non-Cryst. Solids, 2011, 357, 1328-1334.

[17] Efimov, A. M., "IR fundamental spectra and structure of pyrophosphate glasses along the $2ZnO·P_2O_5$-$2Me_2O·P_2O_5$ join (Me being Na and Li)", J. Non-Cryst. Solids, 1997, 209, 209-226.

[18] Paulose, P. I., Jose, G., Unnikrishnan, N. V., "Energy transfer studies of Ce:Eu system in phosphate glasses", J. Non-Cryst. Solids, 2010, 356, 93-97.

[19] Efimov, A. M., Pogareva, V. G., "Water-related IR absorption spectra for some phosphate and silicate glasses", J. Non-Cryst. Solids, 2000, 275, 189-198.

[20] Liu, H. S., Chin, T. S., Yung. S. W., "FTIR and XPS studies of low-melting PbO-ZnO-P_2O_2 glasses", Mater. Chem. Phys., 1997, 50, 1-10.

[21] Buyn, J. O., Kim, B. H., Hong, K. S., Jung, H. J., Lee, S. W., Izyneev, A. A., "Properties and structure of RO-Na_2O-Al_2O_3-P_2O_5 (R= Mg, Ca, Sr, Ba) glasses", J. Non-Cryst. Solids, 1995, 190, 288-295.

[22] Corbridge, D. E. C., "Topics in Phosphorus Chemistry", lnterscience, New York, 1969, 6, 232.

[23] Rulmont A., Cahay R., Liegeois-Duyckaerts M., Tarte P., "Vibrational spectroscopy of phosphate: Some general correlations between structure and spectra", Eur. J. Solid State Inorg. Chem., 1991, 28, 207-219.

[24] Sales, B. C., Otaigbe, J. U., Beall, G. H., Boatner, L. A., Ramey, J. O., "Structure of zinc polyphosphate glasses", J. Non-Cryst. Solids, 1998, 226, 287-293.

[25] Hruby, A., "Evaluation of glass-forming tendency by means of DTA", Czech J. Phys. B 1972, 22, 1187-1193.

[26] Mott, N. F., "Conduction in glasses containing transition metal ions" J. Non-Cryst. Solids, 1968, 106, 1-17.

[27] Austin, I. G., Mott, N. F., "Polarons in Crystalline and Non Crystalline Materials" Adv. Phys., 1969, 18, 41-102.

[28] Jiang, J, Zhang, T. J., Zhang, B. S., Mao,

H, "Complex impedance analysis of $Ba_{0.65}Sr_{0.35}TiO_3$ ceramics" J. Electroceram., 2008, 21, 258-262.

[29] Liu, J., Duan, C. G., Yin, W. G., Mei, W. N., Smith, R. W., Hardy, J. R., "Dielectric permittivity and electric modulus in Bi2Ti4O11" J. Chem. Phys., 2003, 119, 2812-2819.

[30] Bonneau, P, Garnier, O, Calvarin, G, Husson, E, Gahvarri, J. R., Hewat, A. W., Morrel, A, "X-ray and neutron diffraction studies of the diffuse phase transition in $PbMg_{13}Nb_{23}O_3$ ceramics". J. Solid State Chem., 1991, 91, 350-361.

[31] Jorcin, B, Orazem, M. E., Pebere, N, Tribollet, B, "CPE analysis by local electrochemical impedance spectroscopy". Electrochim. Acta, 2006, 51, 1473-1479.

[32] Komornicki, S, Radecka, M, Rekas, M, "Frequency-dependent electrical properties in the system SnO_2-TiO_2". J. Mater. Sci., 2001, 12, 11-16.

[33] Ben Said, R, Louati, B, Guidara, K, "Electrical properties and conduction mechanism in the sodium nickel diphosphate". Ionics, 2014, 20, 703-711.

[34] Khelifi, H, Zouari, I, Al-Hajry, A, Abdelmoula, N, Mezzane, D, Khemakhem, H, "Ac conductivity and ferroelectric phase transition of $Bi_{0.7}(Ba_{0.8}Sr_{0.2})_{0.3}Fe_{0.7}Ti_{0.3}O_3$ ceramic". Ceram., 2015, 41, 12958-12966.

[35] Sdiri, N, Elhouichet, H, Elakermi, E, Dhifallah, A, Ferid, M, "Structural investigation of amorphous $Na_2O - P_2O_5 - B_2O_3$ correlated with its ionic conductivity". J. Non-Cryst. Solids, 2015, 409, 34-42.

[36] Sdiri, N, Elhouichet, H, Azeza, B, Mokhtar, F, "Studies of $(90\text{-}x)P_2O_{5x}B_2O_310Fe_2O_3$ glasses by Mossbauer effect and impedance spectroscopy methods". J. Non-Cryst. Solids, 2013, 371-372, 22-27.

[37] Šantić, A, Moguš-Milanković, A, "Charge Carrier Dynamics in Materials with Disordered Structures: A Case Study of Iron Phosphate Glasses". Croat. Chem. Acta, 2012, 85(3), 245-254.

[38] Langar, A, Sdiri, N, Elhouichet, H, Ferid, M, "Conductivity and dielectric behavior of $NaPO_3 - ZnO - V_2O_5$ glasses". J. Alloys Compd., 2014, 590, 380-387.

[39] Suzuya, K, Itoh, K, Kajinami, A, Loong, C. K., "The structure of binary zinc phosphate glasses". J. Non-Cryst Solids, 2004, 345-346, 80-87.

[40] Saroj, R, Sujata, S, Neetu, A, Ashish, A, "Crystallization kinetics, optical and dielectric properties of $Li_2O{\cdot}CdO{\cdot}Bi_2O_3{\cdot}SiO_2$ glasses". J. Mol Struct., 2015, 1098, 1-11.

[41] Rani, S, Sanghi, S, Agarwal, A, Ahlawat, N, "Effect of Bi_2O_3 on the dynamics of Li^+ ions in $Li_2O.P_2O_5$ glasses". J. Mater Sci., 2009, 44, 5781-5787.

[42] Eraiah, B, Anavekar, R. V., "DC electronic conductivity studies on zinc vanadophosphate glasses". Phys. Chem. Glasses, 2001, 42, 121-125.

[43] Devidas, G. B., Sankarappa, T, Chougule, B. K., Prasad, G, "DC conductivity in single and mixed alkali vanadophosphate glasses". J. Non Cryst. Solids, 2007, 353, 426-434.

[44] Garbarczyk, J. E., Machowski, P, Wasiucionek, M, Tykarski, L, Bacewicz, R, Aleksiejuk, A, "Studies of silver-vanadate-phosphate glasses by Raman, EPR and impedance spectroscopy methods". J. Solid State Ion., 2000, 136-137, 1077-1083.

[45] Jayasinghe, G. D. L. K., Dissanayake, M. A. K. L., Careem, M. A., Souquet, J. L., "Electronic to ionic conductivity of glasses in the Na_2O-V_2O_5-TeO_2 system". Solid State Ion., 1997, 93, 291-295.

[46] Jayasinghe, G. D. L. K., Bandaranayake, P. W. S. K., Souquet, J. L., "Mixed former effect in sodium phospho tellurate glasses". Solid State Ion., 86-88, 1996, 447-451.

[47] El-Desoky, M. M., "Characterization and transport properties of V_2O_5-Fe_2O_3-TeO_2 glasses". J. Non Cryst. Solids, 2005, 351, 3139-3146.

[48] Christensen, R, Olson, G, Martin, S. W., "Structural Studies of Mixed Glass Former $0.35Na_2O + 0.65[xB_2O_3 + (1\text{-}x)P_2O_5]$ Glasses by Raman and 11B and 31P Magic Angle Spinning Nuclear Magnetic Resonance Spectroscopies". J. Phys. Chem., 2013, 117, 2169-2179.

[49] Dhote, D. S., "Transport properties of vanadium borate glasses". Int. Res. J. Sci. Eng., 2014, 2, 161-166.

[50] Al-Hajry, A, Al-Shahrani, A, El-Desoky, M. M., "Structural and other physical properties of barium vanadate glasses". Mater. Chem. Phys., 2006, 95, 300-306.

[51] Thangadurai, V, Weppner, W, "Solid state lithium ion conductors: Design considerations by thermodynamic approach". Ionics, 2002, 8, 281-292.

[52] Thombre, M. D., "Study of Physical Properties of Sodiumborophosphate Glasses". Indian J. Appl. Re., 2014, 4, 469-472.

[53] Ong, S. P., Mo, Y, Ceder, G, "Low hole polaron migration barrier in lithium peroxide". Phys. Rev. B, 2012, 85, 081105(R).

[54] Montani, R. A., Lorente, A, Vincenzo, M. A., "Effect of Ag_2O on the conductive behaviour of silver vanadium tellurite glasses". Solid State Ion., 2000, 130, 91-95.

[55] Abid, M, Et-tabirou, M, Hafid, M, "Glass forming region, ionic conductivity and infrared spectroscopy of vitreous sodium lead mixed phosphates". Mater. Res. Bull., 2001, 36, 407-421.

[56] Sokolov, I. A., Tarlakov, Y. P., Ustinov, N. Y., Pronkin, A. A., "Structure and Electric Properties of Lithium Phosphate Glasses". Russ. J. Appl. Chem., 2005, 78 (5), 741-746.

[57] Khor, S. F., Talib, Z. A., Daud, W. M., Sidek, H. A. A., Ng, B. H., "Effects of MgO on dielectric properties and electrical conductivity of ternary zinc magnesium phosphate glasses". J. Non-Cryst. Solids, 2009, 355, 2533-2539.

[58] Bale, S, Rahman, S, "Role of ZnO in Dc Electrical Conductivity of Lithium Bismuthate Glasses". ISRN Mater. Sci., 2013, 1-9.

[59] Sdiri, N, Elhouichet, H, Dhaou, H, Mokhtar, F, "Effects of the substitution of P_2O_5 by B_2O_3 on the structure and dielectric properties in $(90\text{-}x)P_2O_5\text{-}xB_2O_3\text{-}10Fe_2O_3$ glasses". Spectrochim. Acta A Mol. Biomol. Spectrosc., 2014, 117, 309-314.

[60] Graça, M. P. F., Valente, M. A., Ferreira da Silva, M. G., "Electrical properties of lithium niobium silicate glasses". J. Non-Cryst. Solids, 2003, 325, 267-274.

[61] Bouzidi, C, Sdiri, N, Boukhachem, A, Elhouichet, H, Ferid, M, "Impedance analysis of $BaMo_{1-x}W_xO_4$ ceramics". Superlattices and Microstruct., 2015, 82, 559-573.

[62] Schütt, H. J., "A new phenomenological description of the electrical relaxation in ionic conductors". Solid. State. Ion., 1994, 72, 86-88.

[63] Hodge, L. M., Angell, C. A., "Electrical relaxation in amorphous protonic conductors". J. Chem. Phys., 1977, 67, 1647-1658.

[64] James, A. R., Prakash, C, Prasad, G, "Structural properties and impedance spectroscopy of excimer laser ablated Zr substituted $BaTiO_3$ thin films". J. Phys. D. Appl. Phys., 2006, 39, 1635-1641.

[65] Bahgat, A. A., Abou-Zeid, Y. M., "Mixed alkali effect in the $K_2O\text{-}Na_2O\text{-}TeO_2$ glass system". J. Phys. Chem. Glasses, 2001, 42, 361-370.

[66] Gedam, R. S., Ramteke, D. D., "Electrical, dielectric and optical properties of La_2O_3 doped lithium borate glasses". J. Phys. Chem. Solids, 2013, 74, 1039-1044.

[67] Sidebottom, D. L., "Influence of cation constriction on the ac conductivity dispersion in metaphosphate glasses". Phys. Rev. B, 2000, 61, 14507-14516.

[68] Gerhardt, R. A., "Impedance and dielectric spectroscopy revisited: distinguishing localized relaxation from long-range conductivity". J. Phys. Chem. Solids, 1994, 55, 1491-506.

[69] Onwudiwe, D. C., Arfin, T, Strydom, C. A., "Surfactant mediated synthesis of ZnO nanospheres at elevated temperature, and their dielectric properties". Superlattices. Microstruct., 2015, 81, 215-225.

[70] Martin, S. W., Angell, C. A., "Dc and ac conductivity in wide composition range $Li_2O\text{-}P_2O_5$ glasses". J. Non-Cryst. Solids, 1986, 83, 185-207.

[71] Ben Rhaiem, A, Hlel, F, Guidara, K, Gargouri, M, "Dielectric relaxation and ionic conductivity studies of $[N(CH_3)_4]2Cu_{0.5}Zn_{0.5}Cl_4$". J. Alloy Compd., 2008, 463, 440-445.

[72] Dutta, A, Sinha, T. P., Jena, P, Adak, S, "Ac conductivity and dielectric relaxation in ionically conducting soda-lime-silicate glasses". J. Non-Cryst. Solids, 2008, 354,

3952-3957.

[73] Saha, S, Sinha, T. P., "Low-temperature scaling behavior of $BaFe_{0.5}Nb_{0.5}O_3$". Phys. Rev. B, 2002, 65, 1341031-1341037.

[74] Ganguly, P, Jha, A. K., "Impedance spectroscopy analysis of $Ba_5NdTi_3Nb_7O_{30}$ ferroelectric ceramic". Physica B, 2010, 405, 3154-3158.